Uncalcined TS-2 Immobilized Au Nanoparticles as a Bifunctional Catalyst to Boost Direct Propylene Epoxidation with H_2 and O_2

Zhihua Zhang[a], Xuan Zhao[a], Gang Wang[a], Jialun Xu[a], Mengke Lu[a], Yanqiang Tang[a], Wenzhao Fu[a], Xuezhi Duan[a,*], Gang Qian[a], De Chen[b], Xinggui Zhou[a,*]

[a] State Key Laboratory of Chemical Engineering, East China University of Science and Technology, Shanghai 200237, China

[b] Department of Chemical Engineering, Norwegian University of Science and Technology, Trondheim 7491, Norway

[*] Corresponding authors: xzduan@ecust.edu.cn; xgzhou@ecust.edu.cn

Tel.: +86-21-64250937; Fax.: +86-21-64253528

Abstract:

Developing stable yet efficient Au-Ti bifunctional catalysts is important but challenging for direct propylene epoxidation with H_2 and O_2. This work describes a novel strategy of employing uncalcined titanium silicalite-2 (TS-2-B) to immobilize Au nanoparticles as a bifunctional catalyst for the reaction. Under no promoter effects, the Au/TS-2-B catalyst compared to the referenced Au/TS-1-B catalyst delivers outstanding catalytic performance, i.e., exceptionally high stability over 100 h, propylene oxide (PO) formation rate of 118 $g_{PO}\cdot h^{-1}\cdot kg_{cat}^{-1}$, PO selectivity of 90% and hydrogen efficiency of 35%. The plausible relationship of catalyst structure and performance is established by using multiple tehniques, such as UV-vis, HAADF-STEM, TGA and XPS. A unique synergy of Au-Ti^{4+}-Ti^{3+} triple sites is proposed for our developed Au/TS-2-B catalyst with the higher stable PO formation rate and hydrogen efficiency.The insights reported here could shed new light on the rational design of highly stable and efficient Au-Ti bifunctional catalysts for the reaction.

Keywords: propylene epoxidation, Au/TS-2, bifunctional catalyst, high stability, hydrogen efficiency

Introduction

Probing the Ti-containing materials for Au dispersion and immobilization is of scientific and industrial importance for direct propylene epoxidation with H_2 and O_2, which is sustainable and highly efficient synthesis of propylene oxide (PO).[1-3] There is a consensus that the reaction proceeds by means of bifunctional catalysis, i.e., the reaction of H_2 with O_2 on the Au surfaces to produce hydroperoxy species followed by transport of such species to nearby isolated Ti sites to form active Ti-OOH intermediates toward oxidation of the adsorbed propylene to form PO,[4-7] and the isolated Ti^{4+}-rich TS-1 immobilized Au catalysts show state-of-the-art PO formation rates.[1,8-17] Recently, uncalcined TS-1 with blocked micropores (TS-1-B) has been employed to immobilize Au catalysts for suppressing the catalyst deactivation from the micropore blocking by carbon deposits and keeping a relatively stable activity for ~ 30 h.[15] As a consecutive effort, it is highly desirable to develop more stable yet highly active Au-Ti bifunctional catalysts for the targeted reaction.

Deposition-precipitation (DP) method based on the isoelectric point principle is an effective way to selectively deposit Au nanoparticles nearby the active isolated Ti^{4+} sites for preparing Au-Ti bifunctional catalysts.[13,18-21] The precipitant agent using urea has shown much higher Au capture efficiency on the uncalcined titaniumsilicates (e.g., TS-1-B) than that using NaOH or Na_2CO_3 (< 3 %) due to the formation of different gold species.[13,14,22-24] In addition, the former method can also avoid introducing alkaline ions such as Na^+, which have been reported to remarkably affect the reaction.[12,25-33] Therefore, employing DP urea (DPU) method to prepare Au-Ti bifunctional catalysts is highly desirable to understand the underlying nature of the Au-Ti synergistic effects without the interference of the residual alkaline metal effects.

For the above used titaniumsilicates, the isolated Ti^{4+} sites are mainly responsible for the PO formation, but their acidic characteristic has a detrimental effect on the PO selectivity, promoting

PO ring-opening side reaction to generate carbonaceous deposits and causing gradual catalyst deactivation.[20,34-40] In addition to the isolated Ti^{4+} sites, another Ti species, i.e., the defective Ti^{3+} sites, are also observed, which are suggested to be active for H_2O_2 activation to generate hydroxyl radicals and superoxo species which can enhance the elimination of the carbonaceous deposits.[41-47] This indicates the significant importance of employing titaniumsilicates with appropriate composition and properties of Ti species for development of highly stable yet active Au-Ti bifunctional catalysts for the reaction. Along this line, an attempt is urgently made to employ another isolated Ti^{4+}-rich, titanium silicate-2 (TS-2),[48,49] having different crystallization mechanism against TS-1 and thus more defective Ti^{3+} sites, for immobilizing Au nanoparticles toward development of industrially attractive Au/TS-2-B bifunctional catalyst for the reaction.

The objective of this study is to develop more stable yet highly active Au-Ti bifunctional catalysts for the reaction by employing uncalcined TS-2 (i.e., TS-2-B) to immobilize Au nanoparticles using the DPU method. This method avoids introducing the alkaline ions, which makes it easier to understand the underlying nature of the Au-Ti synergistic effects without the interference of the promoter effects. The catalytic behaviors of our developed Au/TS-2-B catalyst and the referenced Au/TS-1-B catalyst were comparatively studied. Structural and/or electronic properties of titaniumsilicates as well as fresh and used catalysts were characterized by multiple techniques, such as UV-vis, HAADF-STEM, TGA and XPS. Finally, a plausible catalyst structure-performance relationship was established, and a unique synergy of Au-Ti^{4+}-Ti^{3+} triple sites was proposed for our developed Au/TS-2-B catalyst with the higher stable PO formation rate and hydrogen efficiency.

Experimental

Synthesis of Au/TS-2-B catalyst and the referenced Au/TS-1-B catalyst

Uncalcined titanium silicalite-2 (TS-2-B) was hydrothermally synthesized according to the method reported previously in the literature.[50] Because the hydrolysis of tetraethylorthosilicate (TEOS) is much slower than that of titanium (IV) tetrabutoxide (TBOT), the TEOS was firstly added into the tetrabutylammonium hydroxide (TBAOH) solution followed by dropwise addition of the TBOT dissolved in isopropanol (IPA), where the molar ratio of TEOS, TBOT and TBAOH is 1: 0.01: 0.15. The resultant solution was transferred into Teflon autoclave at 180 ºC for 48 h. The as-synthesized TS-2 was completely washed and then dried overnight at room temperature in a vacuum oven. Similarly, uncalcined titanium silicalite-1 (TS-1-B) with the same Si/Ti molar ratio was also synthesized except using tetrapropylammonium hydroxide (TPAOH) to replace TBAOH as the template agent. The Au/TS-2-B catalyst and the referenced Au/TS-1-B catalyst with the same gold loading of ~0.09 wt% were prepared via the DPU method according to the procedure previously reported,[22] where the gold loadings of the two catalysts were determined by inductive coupled plasma atomic emission spectrometry (ICP-AES, IRIS 1000).

Catalyst characterization

X-ray diffraction (XRD) patterns were recorded using a Rigaku D/Max2550VB/PC diffractometer equipped with a Cu K_{α} radiation. Ultraviolet-visible spectroscopy (UV-vis) was conducted on a PerkinElmer Lambda 35 spectrophotometer with a $BaSO_4$ plate as the reference. High-angle annular dark-field scanning transmission electron microscopy (HAADF-STEM) was performed on a Tecnai G2 F20 S-Twin equipped with a digitally processed STEM imaging system. Scanning electron microscopy (SEM) images were taken using a NOVA Nano SEM450 microscope (FEI, USA) operating at 3 kV. High-resolution transmission electron microscopy (HRTEM) images were taken using a JEM 2100 instrument (JEOL, Japan) operating at 200 kV.

N_2 adsorption-desorption measurements were performed at 77 K using an ASAP 2020 instrument (Micromeritics, USA). Thermogravimetric analysis (TGA) was performed on a PerkinElmer TGA Pyris 1 by heating dried sample from room temperature to 800 °C in a flow of N_2/O_2 = 8:1 with a ramping rate of 10·°C min^{-1}. X-ray photoelectron spectroscopy (XPS) was performed on a Kratos Axis XSAM-800 instrument using Al K_α X-ray with 1486.6 eV as the excitation source, and the internal standard of the C 1s peak was set as 284.6 eV.

Catalytic testing

The Au/TS-2-B and referenced Au/TS-1-B catalysts were tested for direct propylene epoxidation with H_2 and O_2 in a fixed-bed quartz reactor with an inner diameter of 8 mm under atmospheric pressure. The catalysts (~ 0.15 g) were in-situ reduced in the reactor, the temperature was raised from room temperature to 200 °C with a heating rate of 1 °C·min^{-1} in a stream (48 mL·min^{-1}) of 30 vol % H_2 in N_2. Subsequently, feed gas containing C_3H_6, O_2, H_2 and N_2 with volume ratio of 1:1:1:7 at a flow rate of 35 mL·min^{-1} was passed through the reactor, and then the catalytic testing was started. The reactants and products were analyzed by an on-line gas chromatograph (GC) equipped with thermal conductivity detector (TCD) and flame ionization detector (FID). Oxygenates such as propylene, acetaldehyde, PO, acetone, acrolein and propanal were separated using a PLOT Q capillary column (0.35 mm ×30 m) and analyzed via FID. The hydrogen, oxygen and CO_2 were separated using a Porapak T packed column (3 mm × 1 m) and analyzed via TCD, where N_2 was used as the carrier gas due to good H_2 signal.[12,13,17] The propylene conversion, PO selectivity and hydrogen efficiency were calculated as follows:

Propylene conversion = moles of (C_3-oxygenates + 2/3 ethanal +1/3 CO_2) / moles of propylene in the feed.

PO selectivity = moles of PO / moles of (C_3-oxygenates + 2/3 ethanal +1/3 CO_2)

Hydrogen efficiency = moles of PO / moles of hydrogen converted

Results and Discussion

Outstanding performance of the Au/TS-2-B catalyst

The crystal structures and Ti species of the as-synthesized TS-2 together with our previously obtained uncalcined TS-1 were characterized by XRD and UV-vis, respectively, where the uncalcined TS-1 was used as a reference to understand the underlying nature of the synergy between the uncalcined titaniumsilicalites and Au nanoparticles for direct propylene epoxidation with H_2 and O_2. Figure 1a shows XRD patterns of the two samples, which are indicative of typical diffraction peaks of TS-2-B and TS-1-B, respectively.[15,17,50] It can be clearly seen in Figure 1b that both samples present the main absorption bands around 210 nm, assigned to be isolated tetrahedrally coordinated Ti (i.e., Ti^{4+}) species substitution into the zeolite framework, which indicates similar Ti species in the TS-2-B and TS-1-B.[15,17,50,51] These two uncalcined titaniumsilicalites were then employed to immobilize Au nanoparticles for the synthesis of Au/TS-2-B and Au/TS-1-B bifunctional catalysts. As shown in Figure 1c and 1d, these two catalysts exhibit similar Au average particle sizes, i.e., 2.9 nm for the Au/TS-2-B catalyst and 2.6 nm for the Au/TS-1-B catalyst.

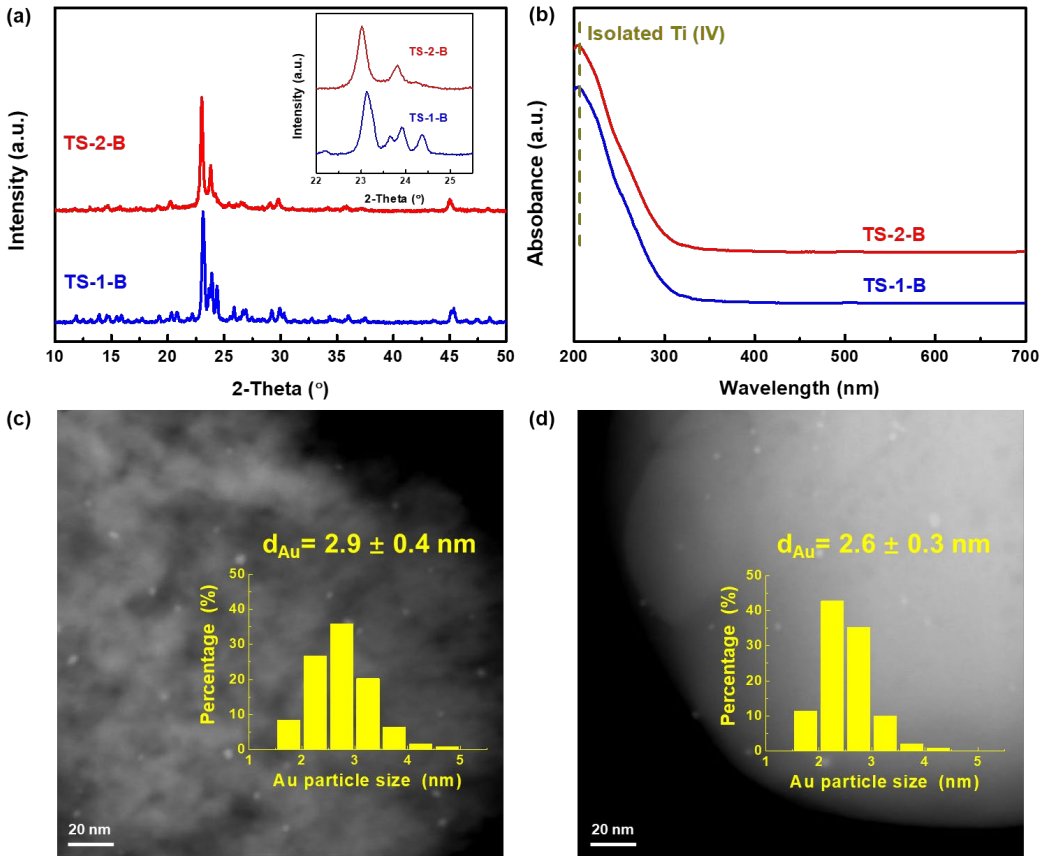

Figure 1. (a) XRD patterns and (b) UV-vis spectra of TS-2-B and TS-1-B. Representative HAADF-STEM images and the corresponding Au particle size distributions of Au/TS-2-B (c) and Au/TS-1-B (d) catalysts.

Subsequently, the two Au/TS-2-B and Au/TS-1-B bifunctional catalysts with similar Au nanoparticle sizes and typed Ti species were tested for direct propylene epoxidation with H_2 and O_2, and the results are shown in Figure 2a. Unexpectedly, these two catalysts exhibit significantly different catalytic behaviors. As the reaction proceeds, the Au/TS-1-B catalyst is found to undergo a short induction period of 3 h followed by a decline to a steady state, where the stable PO formation rate is 71 $g_{PO}{\cdot}h^{-1}{\cdot}kg_{cat}^{-1}$. However, the Au/TS-2-B catalyst undergoes much longer induction period of 18 h and then reaches high stable PO formation rate, i.e., 118 $g_{PO}{\cdot}h^{-1}{\cdot}kg_{cat}^{-1}$, over 100 h, 1.6 times higher than that of the referenced Au/TS-1-B catalyst. This

indicates that the TS-2 could be a better candidate to prepare more stable yet highly efficient bifunctional catalyst for the reaction.

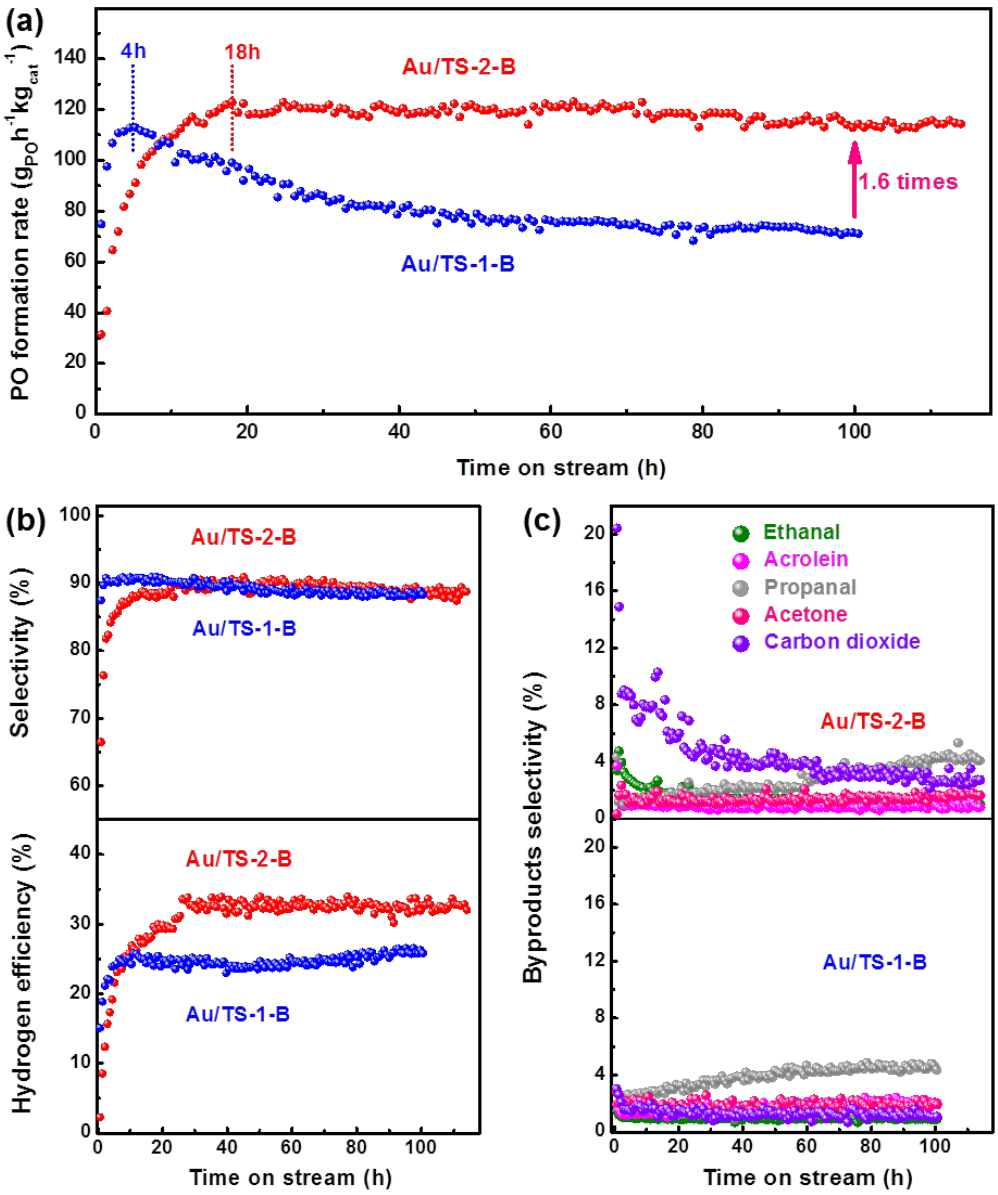

Figure 2. (a) PO formation rate, (b) PO selectivity and hydrogen efficiency as well as (c) byproducts selectivity as a function of time on stream over Au/TS-2-B and Au/TS-1-B catalysts.

In addition to the activity, the products selectivity of the two catalysts is another important issue. It can be clearly observed in Figures 2b and 2c that in the initial induction period, the

Au/TS-2-B catalyst exhibits much lower selectivity to PO but much higher selectivty to CO_2 and ethanal than the Au/TS-1-B catalyst. This indicates the occurrence of C-C bond cleavage, possibly resultant from the further cracking reactions of PO.[17,22,39] After the induction period, the two catalysts give rise to relatively high selectivity to PO as well as the suppression of the C-C bond cleavage, where the Au/TS-2-B catalyst shows higher selectivity to PO compared to the Au/TS-1-B catalyst. Additionally, during the whole reaction process, there are little change in the selectivity to acetone and acrolein, but gradually increased selectivity to propanal.

Moreover, the hydrogen efficiency is also a key aspect for this reaction system, because it determines such process viability and economy. According to previous studies,[12,13,17,26,52,53] there are two kinds of definitions for the hydrogen efficiency: one is the ratio of the moles of PO produced to those of H_2 converted, the other is the ratio of the moles of PO to those of H_2O formed. As shown in Scheme 1, in addition to the main reactions to form PO, there also exist some side-reactions including hydrogenation of propylene to propane, oxidation of propylene to acrolein, isomerization of PO to propanal and acetone as well as oxidative cracking of PO to CO_2 and ethanal.[39,54] In our cases, i.e., the direct epoxidation of propylene with H_2 and O_2 over the Au/TS-2-B and Au/TS-1-B catalysts, no propane signal was detected by GC, and the formation of acrolein, ethanal and CO_2 side-products accompanies with that of water resultant from the propylene and PO, which would lead to the under-estimation of the hydrogen efficiency calculated by the second definition. These analyses suggest that the hydrogen efficiency calculated by the first definition is more reasonable. This can be supported by the comparison between the hydrogen efficiency calculated by the first definition and that calculated by the second definition leading to the over-estimated hydrogen efficiency, where more details are shown in Supporting Information, Table S1, Figure S1 and Figure S2.

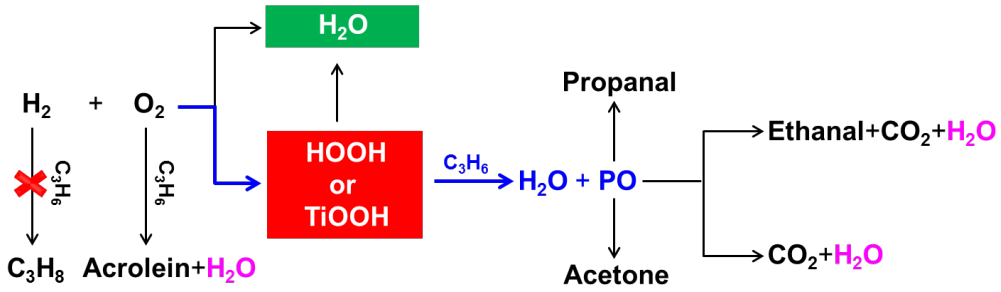

Scheme 1 Plausible reaction pathways of direct propylene epoxidation with H_2 and O_2. In our cases, over the Au/TS-2-B and Au/TS-1-B catalysts, no propane signal was detected by GC.

Notably, Delgass et al. reported that the 0.09 wt% Au/TS-1-B (d_{Au} > 5.3 nm and Si/Ti molar ratio =119) prepared by DP method using Na_2CO_3 as precipitation agent exhibits a hydrogen efficiency of 18.2 %,[17] and our previous work showed that the 0.10 wt% Au/TS-1-B (d_{Au} = ca. 3.3 nm and Si/Ti molar ratio = 100) prepared by DP method using NaOH as precipitation agent catalyst exhibits that of 19.5 %.[15] This relatively high hydrogen efficiency of the latter catalyst could be realted to the smaller Au particle size and lower Si/Ti molar ratio.[1,15] Along this line, it is easy to understand that the 0.09 wt% Au/TS-1-B catalyst (d_{Au} = ca. 2.6 nm and Si/Ti molar ratio = 100) prepared by DPU method has high hydrogen efficiency of ca. 25%. As mentioned in the Introduction, when employing the DP method with using Na_2CO_3 or NaOH as precipitation agent, there would exist the interference of the residual alkaline ions. Probing the effects of the preparation method is an interesting yet important subject, which is still ongining in our group. More interestingly, when the TS-2-B was used to immobilize Au nanoparticles by DPU method, the resultant 0.09 wt% Au/TS-2-B catalyst (d_{Au} = ca. 2.9 nm and Si/Ti molar ratio = 100) gives rise to much higher hydrogen efficiency of 35%. On the one hand, the Au/TS-2-B and Au/TS-1-B catalysts have similar gold loadings but remarkably different surface area in Table S2, and thus remarkably different population density of Au nanoparticls, which could be one reason for the much higher hydrogen efficiency of the 0.09 wt% Au/TS-2-B catalyst.[1] On the other hand, the

appropriate catalyst electronic properties of the Au/TS-2-B catalyst may be another reason for the much higher hydrogen efficiency, which will be discussed in detail later.

Remarkably different induction periods over the two catalysts

The microstructures of the two uncalcined titaniumsilicates, i.e., the TS-2-B and TS-1-B, were first characterized by SEM and HRTEM-SAED, and the results are shown in Figure 3. It can be clearly seen in Figure 3a and 3c that the TS-2-B displays a fusiform-like shape with rough external surfaces. Additionally, the higher resolution image (Figure 3e) also reveals that the TS-2-B particles are composed of large numbers of small-sized zeolite. The SAED pattern for TS-2-B (Figure 3g) shows that these small-sized zeolites are orientated along the same crystalline axis, which is similar to the case of orientated nano-zeolite aggregates obtained in the previous work.[55,56] Moreover, as shown in Figure 3b and 3d, the TS-1-B exhibits a coffin-like shape with smooth external surfaces, and Figure 3f and 3h exhibit that TS-1-B possesses well defined edges and a SAED pattern with bright spots, which evidences the single-crystalline nature of TS-1-B.[57] The textural properties of the two uncalcined titaniumsilicates were further characterized by N_2 physisorption, and the results are shown in Figure 3i as well as Table S2. As obviously observed in Figure 3i, compared to the TS-1-B, the TS-2-B shows typical type IV isotherm with a H3 hysteresis loop,[55] which is indicative of mesoporous characteristic, leading to a most probable pore size of ca. 12.5 nm. Such mesoporous characteristic is most likely due to the aggregation of small-sized zeolite, as evidenced by the randomly distributed white fields throughout the whole crystal (Figure 3e).[58] In contrast, no mesopores exist in TS-1-B sample. Moreover, taking into account the characteristics of the DP urea method involving acidic-basic environments, its effects on the textural properties of the two fresh Au-Ti bifunctional catalysts, i.e., the Au/TS-2-B and Au/TS-1-B catalysts, were probed by N_2 physisorption. As shown in Figure 3i, there are

no legible changes in the textural properties. All of these results almost guarantee that under the present catalyst preparation conditions, employing uncalcined titaniumsilicates can allow the deposition of Au nanoparticles on their external surfaces.

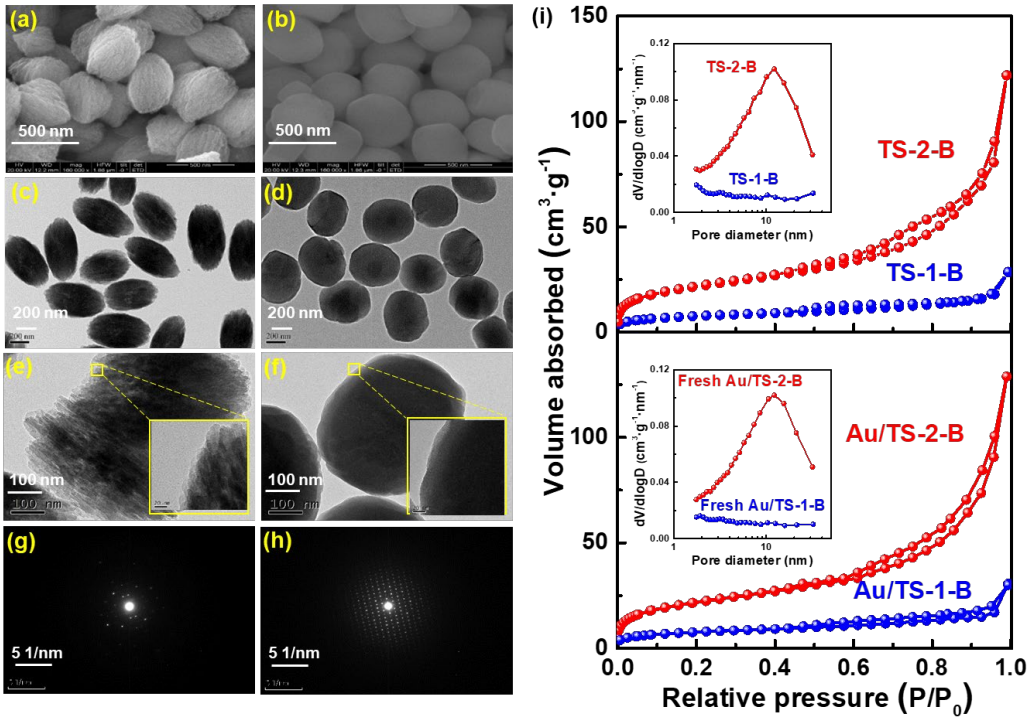

Figure 3. Representative SEM images, HRTEM images and SAED patterns of TS-2-B (a, c, e and g) and TS-1-B (b, d, f and h), respectively. (i) N_2 adsorption-desorption isotherms and pore size distributions of TS-2-B and TS-1-B as well as fresh Au/TS-2-B and Au/TS-1-B catalysts.

Evaluating of the thermal behaviors over the two catalysts is of crucial importance, because the usage of uncalcined titaniumsilicates may bring about the interference of released template agents arising from the fresh Au-Ti bifunctional catalysts with residual template agents on the external surfaces and inside the micropores during the practical reaction system. Along this line, TGA measurements were carried out, and the results are shown in Figure 4a. The two catalysts are observed to exhibit legible weight loss lower than 330 ^{o}C and remarkable weight loss higher

than 350 °C, which are possibly ascribed to the decomposition of templates on the external surfaces and those in the micropores, respectively.[48,49,59]

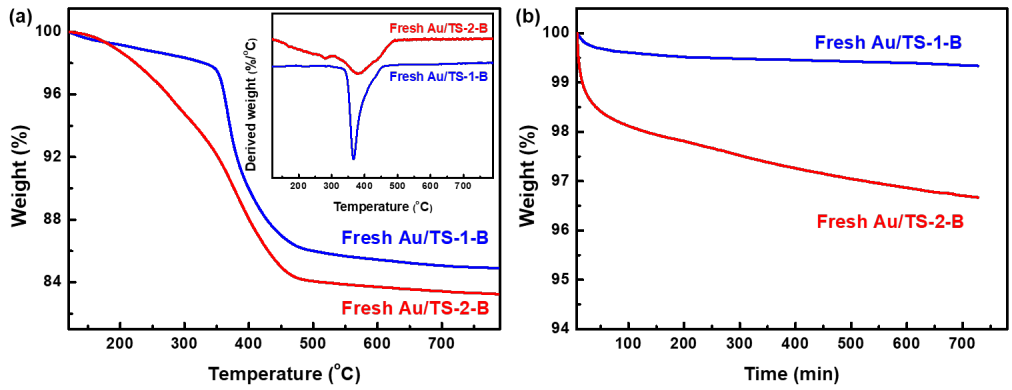

Figure 4. (a) TG and DTG analysis profiles of fresh Au/TS-2-B and Au/TS-1-B catalysts. (b) TG analysis profiles as a function of time of fresh Au/TS-2-B and Au/TS-1-B catalysts at 200 °C.

Notably, considering that the reaction temperature is 200 °C, the thermal behaviors of the two catalysts under such reaction temperature were also studied by TGA. As observed in Figure 4b, the fresh Au/TS-1-B catalyst undergoes a gradual weight loss and then reaches a stable stage after about 3 h, while the fresh Au/TS-2-B catalyst shows a remarkably continuous weight loss within 12 h. These trends could be linked to the significantly different induction periods of the two catalysts mentioned in Figure 2. As the templates release from the catalyst external surfaces, there are more accessible isolated Ti^{4+} active sites. This could provide a rational explanation for the gradually increased PO formation rates for the two catalysts.

During the release of the templates, their effects on the selectivity to different products were also studied. Our preliminary experiments over the two catalysts showed that propylene contact with H_2 is not reactive, but with O_2 can generate trace amount of acrolein. Interestingly, co-feeding propylene, hydrogen and oxygen would significantly enhance the catalytic performance,

because it follows a bifunctional catalysis, i.e., the transport of hydroperoxy species from the reaction of H_2 with O_2 on the Au surfaces to oxidize the nearby isolated Ti sites toward the formation of active Ti-OOH intermediates and subsequent reaction with the absorbed propylene to form the targeted PO.[4-7] However, the formed hydroperoxy species inevitably lead to over-oxidation reactions to generate CO_2 and ethanal, which most likely occur on some specific sites on the titaniumsilicates surfaces.[10,39,40,60,61] As the reaction proceeds, the formation of carbonaceous deposits from PO ring-opening and polymerization side-reactions may block these specific sites and thus suppress the occurrence of the over-oxidation reactions.[30,62] This would give rise to the increased PO selectivity and hydrogen efficiency.

Plausible catalyst structure-stability relationship

In order to understand the above significantly different catalyst stabilities after the induction periods, we resort to multiple catalyst characterization techniques, i.e., HAADF-STEM, TGA and XPS, for obtaining the structural and electronic properties of the two bifunctional catalysts and establishing the plausible catalyst structure-stability relationship.

Previous studies showed that the deactivation of the catalysts mainly originates from the aggregation of the Au nanoparticles and the formation of the carbonaceous deposits.[15,23,25] HAADF-STEM measurements were carried out to probe whether the Au nanoparticles aggregation occurs during the long-term testing. As shown in Figure 5a and 5b, the spent Au/TS-2-B and Au/TS-1-B catalysts give Au average particle sizes of 3.0 and 2.7 nm, respectively, which are similar to the corresponding fresh catalysts in Figure 1c and 1d. This observation indicates that there is no legible aggregation of the Au nanoparticles during the long-term testing. These results indicate that the dramatic difference in the catalytic performance of the two bifunctional catalysts, i.e., a stable and high PO formation rate of the Au/TS-2-B catalyst and

gradual deactivation of Au/TS-1-B catalyst during long-term testing (Figure 2a), may result from the difference in the carbonaceous deposits in the two catalysts.

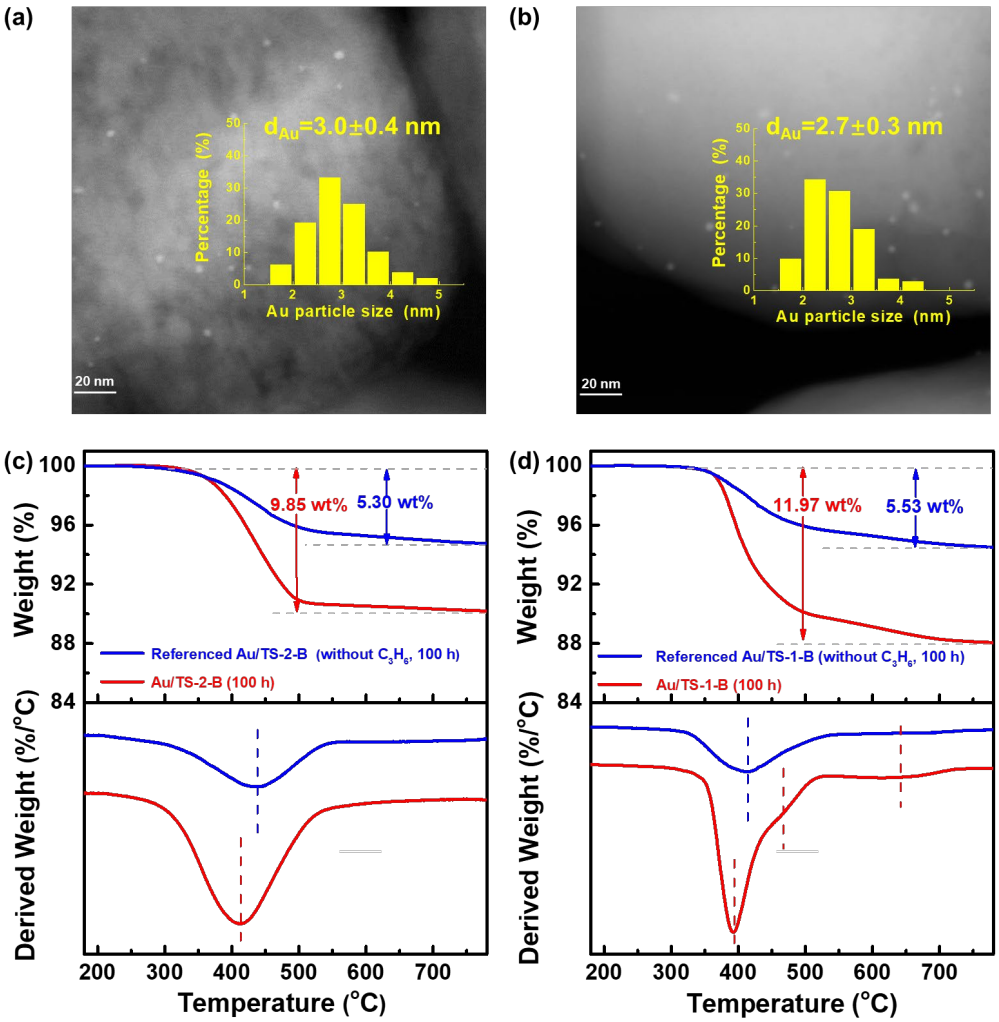

Figure 5. Representative HAADF-STEM images as well as TGA and DTG profiles of spent Au/TS-2-B (a and c) and Au/TS-1-B (b and d) catalysts.

Along this line, TGA measurements were further carried out to investigate the difference in the carbonaceous deposits of the two spent catalysts, and the results are shown in Figure 5c and 5d. To exclude the interference from the possible decomposition of the templates in the micropores during the long-term testing, the fresh Au/TS-1-B and Au/TS-2-B catalysts were

treated under the same reaction conditions without propylene, and the two resultant referenced samples were also analyzed by TGA. From the data shown in Figure 5c and 5d, the amounts of the carbonaceous deposits over the spent catalysts were calculated, and the spent Au/TS-2-B catalyst (i.e., 4.50 wt%) exhibits lower amount of the carbonaceous deposits than the spent Au/TS-1-B catalyst (i.e., 6.40 wt%). Considering the same Au loadings of the two catalysts with the similar Au particle sizes and remarkably different external surface areas (Table S2) of the two titaniumsilicates used here, the two catalysts would exhibit remarkably different Au densities on the titaniumsilicates surfaces. Further combining the same Ti/Si ratios of the two titaniumsilicates used, it could be deduced that these results most likely lead to different electron transfer between Au and titaniumsilicate and thus different properties of the formed carbonaceous deposits over the two catalysts. This deduction would be supported by the analysis of the DTG profiles in Figure 5c and 5d. Clearly, the spent Au/TS-2-B catalyst exhibits one broad DTG peak centered at about 410 ^{o}C, while the spent Au/TS-1-B catalyst with three obvious DTG peaks centered at about 390, 460 and 640 ^{o}C, where the two high-temperature peaks could be attributed to hard coke such as polyalkenes and refractory aromatic species.[35,63] This could provide a rational interpretation for the higher stability of the Au/TS-2-B catalyst because of the suppressed formation of the hard cokes.

To obtain more details about the relationship between the carbonaceous deposits and the catalysts stability, XPS measurements were also performed. Figure 6 shows the Au 4f, Ti 2p and Si 2p spectra and their deconvolution results of fresh Au/TS-2-B and Au/TS-1-B catalysts. Clearly, the Ti 2p and Si 2p binding energies show slight peak shifts over the two catalysts, while the fresh Au/TS-2-B catalyst exhibits higher Au^0 $4f_{7/2}$ binding energy than the fresh Au/TS-1-B catalysts. Notably, the Au 4f spectra were deconvoluted using a non-linear least squares algorithm with a Shirley base line and a Gaussian-Lorentzian combination, and the Au 4f

spectra of the two catalysts both clearly show that the intensity ratio of Au $4f_{5/2}$ and Au $4f_{7/2}$ is 3/4 with a splitting of 3.7 eV, which are well consistent with the characteristic of Au^0 species.[64,65] According to previous theoretical studies,[66-68] the hydrogen dissociation is suggested as rate-determining step in the hydroperoxy species generation on the Au catalysts, and the higher Au binding energy is favourable for the increased Au-H interaction and thus the hydrogen dissociation. These analyses would explain why under the reaction of 18 h, the Au/TS-2-B catalyst exhibits higher stable PO formation rate and hydrogen efficiency than the Au/TS-1-B catalyst.

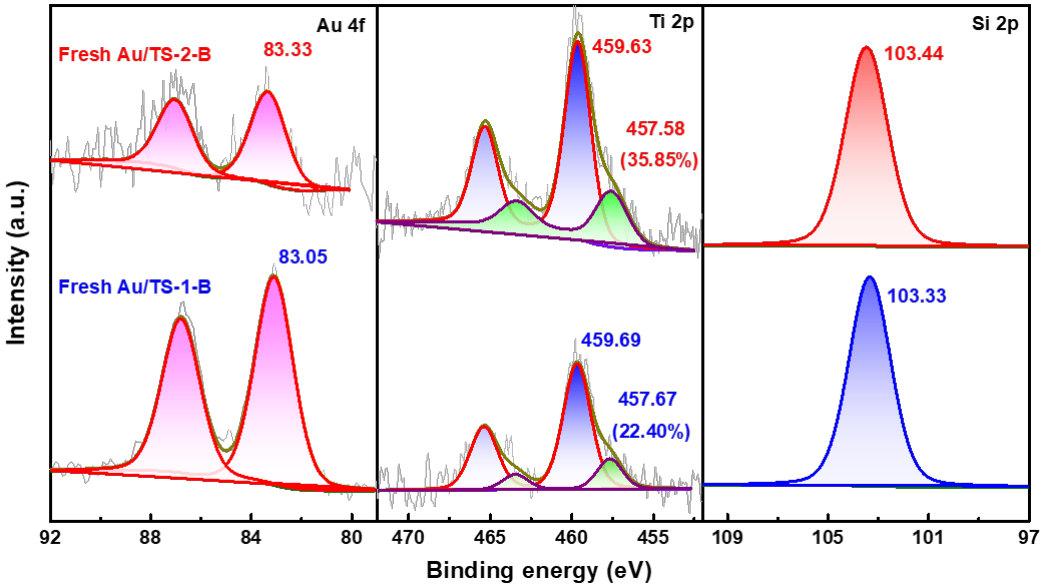

Figure 6. Au 4f, Ti 2p and Si 2p spectra of fresh Au/TS-2-B and Au/TS-1-B catalysts.

Additionally, it has been reported that the materials formed by the attachment of small particles usually generate grain boundaries, which are likely to facilitate the formation of defects.[69-72] According to previous studies,[41-43] the Ti 2p spectra were deconvoluted into Ti^{4+} and Ti^{3+} species, and the results are shown in Figure 6. Obviously, the fresh Au/TS-2-B catalyst exhibits higher Ti^{3+}/Ti^{4+} ratio (based on their XPS peak areas) than the fresh Au/TS-1-B, i.e.,

35.85 % versus 22.40 %. This could be understood by the fact that the TS-2-B is formed by an orientated attachment of small sized crystalline (Figure 3e) and thus the presence of more defects. The Ti^{4+} species are known to be the key to form active Ti-OOH intermediates and thus more targeted PO product,[9,13,20] while the defective Ti^{3+} species are suggested to be active for H_2O_2 activation to form peroxide radicals, which may serve as strong oxidant agents to efficiently eliminate the precursor of hard cokes and thus suppress the formation of hard cokes.[43-47] This could be supported by the phenomena that the Au/TS-2-B catalyst exhibits much higher selectivity to CO_2 than the Au/TS-1-B catalyst, and the former catalyst doesn't show the obvious presence of hard cokes. Therefore, it could be deduced that the synergy of Au-Ti^{4+}-Ti^{3+} triple sites plays an important role in our developed Au/TS-2-B catalyst with the higher stability as well as higher stable PO formation rate and hydrogen efficiency.

Conclusions

In summary, we have successfully developed a stable yet highly active Au/TS-2-B bifunctional catalyst for direct propylene epoxidation with H_2 and O_2 by employing uncalcined TS-2 to immobilize Au nanoparticles using DP urea method. Under no promoter effects, the Au/TS-2-B catalyst compared to the referenced Au/TS-1-B catalyst exhibited longer induction period as well as higher stable PO formation rate and hydrogen efficiency. The presence of the induction period and its remarkable effects on the catalytic performance are attributed to the decomposition of the template absorbed on the external surfaces of the uncalcined titaniumsilicates. The synergy of Au-Ti^{4+}-Ti^{3+} triple sites has been proposed for the Au/TS-2-B catalyst with the higher catalyst stability as well as higher stable PO formation rate and hydrogen efficiency, and the presence of abundant Ti^{3+} could be favorable for suppressing the formation of hard cokes on the catalyst surfaces. These insights demonstrated here could open a new avenue

for the design and optimization of more stable yet highly active Au-Ti bifunctional catalysts for the direct propylene epoxidation with H_2 and O_2.

Acknowledgements

This work was supported by the Natural Science Foundation of China (21922803 and 21776077), the Shanghai Natural Science Foundation (17ZR1407300 and 17ZR1407500), the Program for Professor of Special Appointment (Eastern Scholar) at Shanghai Institutions of Higher Learning, the Shanghai Rising-Star Program (17QA1401200), the Open Project of SKLOCE (SKL-Che-15C03), and the 111 Project of the Ministry of Education of China (B08021).

Literature Cited

1. Huang J, Haruta M. Gas-phase propene epoxidation over coinage metal catalysts. *Res Chem Intermed.* 2012;38:1-24.
2. Qi C. The production of propylene oxide over nanometer Au catalysts in the presence of H_2 and O_2. *Gold Bull*. 2008;41:224-234.
3. Sinha AK, Seelan S, Tsubota S, Haruta M. Catalysis by gold nanoparticles: epoxidation of propene. *Top Catal*. 2004;29:95-102.
4. Bravo-Suárez JJ, Bando KK, Lu J, Haruta M, Fujitani T, Oyama T. Transient technique for identification of true reaction intermediates: Hydroperoxide species in propylene epoxidation on gold/titanosilicate catalysts by X-ray absorption fine structure spectroscopy. *J Phys Chem C.* 2008;112:1115-1123.
5. Huang J, Akita T, Faye J, Fujitani T, Takei T, Haruta M. Propene epoxidation with dioxygen

catalyzed by gold clusters. *Angew Chem Int Ed*. 2009;48:7862-7866.

6. Joshi AM, Delgass WN, Thomson KT. Mechanistic implications of Au_n/Ti-lattice proximity for propylene epoxidation. *J Phys Chem C.* 2007;111:7841-7844.
7. Ji J, Lu Z, Lei Y, Turner CH. Mechanistic insights into the direct propylene epoxidation using Au nanoparticles dispersed on TiO_2/SiO_2. *Chem Eng J*. 2018;191:169-182.
8. Huang J, Takei T, Akita T, Ohashi H, Haruta M. Gold clusters supported on alkaline treated TS-1 for highly efficient propene epoxidation with O_2 and H_2. *Appl Catal B Environ.* 2010;95:430-438.
9. Feng X, Duan X, Yang J, Qian G, Zhou X, Chen D, Yuan W. Au/uncalcined TS-1 catalysts for direct propene epoxidation with H_2 and O_2: Effects of Si/Ti molar ratio and Au loading. *Chem Eng J.* 2015;278:234-239.
10. Feng X, Duan X, Qian G, Zhou X, Chen D, Yuan W. Insights into size-dependent activity and active sites of Au nanoparticles supported on TS-1 for propene epoxidation with H_2 and O_2. *J Catal*. 2014;317:99-104.
11. Huang J, Lima E, Akita T, Guzmán A, Qi C, Takei T, Haruta M. Propene epoxidation with O_2 and H_2: identification of the most active gold clusters. *J Catal.* 2011;278:8-15.
12. Lee WS, Akatay MC, Stach EA, Ribeiro FH, Delgass WN. Enhanced reaction rate for gas-phase epoxidation of propylene using H_2 and O_2 by Cs promotion of Au/TS-1. *J Catal.* 2013;308:98-113.
13. Lee WS, Akatay MC, Stach EA, Ribeiro FH, Delgass WN. Reproducible preparation of Au/TS-1 with high reaction rate for gas phase epoxidation of propylene. *J Catal.* 2012;287: 178-189.
14. Feng X, Duan X, Cheng H, Qian G, Chen D, Yuan W, Zhou X. Au/TS-1 catalyst prepared by deposition–precipitation method for propene epoxidation with H_2/O_2: insights into the effects

of slurry aging time and Si/Ti molar ratio. *J Catal.* 2015;325:128-135.

15. Feng X, Duan X, Qian G, Zhou X, Chen D, Yuan W. Au nanoparticles deposited on the external surfaces of TS-1: enhanced stability and activity for direct propylene epoxidation with H_2 and O_2. *Appl Catal B Environ.* 2014;150:396-401.
16. Feng X, Yang J, Duan X, Cao Y, Chen B, Chen W, Lin D, Qian G, Chen D, Yang C, Zhou X. Enhanced catalytic performance for propene epoxidation with H_2 and O_2 over bimetallic Au-Ag/uncalcined titanium silicate-1 catalysts. *ACS Catal.* 2018;8:7799-7808.
17. Lee WS, Akatay MC, Stach EA, Ribeiro FH, Delgass WN. Gas-phase epoxidation of propylene in the presence of H_2 and O_2 over small gold ensembles in uncalcined TS-1. *J Catal.* 2014;313:104-112.
18. Feng X, Liu Y, Li Y, Yang C, Zhang Z, Duan X, Zhou X, Chen D. Au/TS-1 catalyst for propene epoxidation with H_2/O_2: a novel strategy to enhance stability by tuning charging sequence. *AIChE J.* 2016;62:3963-3972.
19. Feng X, Song Z, Liu Y, Chen X, Jin X, Yan W, Yang C, Luo J, Zhou X, Chen D. Manipulating gold spatial location on titanium silicalite-1 to enhance the catalytic performance for direct propene epoxidation with H_2 and O_2. *ACS Catal*. 2018;8:10649-10657.
20. Taylor B, Lauterbach J, Delgass WN. Gas-phase epoxidation of propylene over small gold ensembles on TS-1. *Appl Catal A Gen*. 2005;291:188-198.
21. Qi C, Akita T, Okumura M, Haruta M. Epoxidation of propylene over gold catalysts supported on non-porous silica. *Appl Catal A Gen*. 2001;218:81-89.
22. Lu X, Zhao G, Lu Y. Propylene epoxidation with O_2 and H_2: a high performance Au/TS-1 catalyst prepared via a deposition-precipitation method using urea. *Catal Sci Technol*. 2013;3:2906-2909.
23. Yap N, Andres RP, Delgass WN. Reactivity and stability of Au in and on TS-1 for

epoxidation of propylene with H_2 and O_2. *J Catal*. 2004;226:156-170.

24. Zanella R, Delannoy L, Louis C. Mechanism of deposition of gold precursors onto TiO_2 during the preparation by cation adsorption and deposition-precipitation with NaOH and urea. *Appl Catal A Gen*. 2005;291:62-72.
25. Lu J, Zhang X, Bravo-Suárez JJ, Fujitani T, Oyama T. Effect of composition and promoters in Au/TS-1 catalysts for direct propylene epoxidation using H_2 and O_2. *Catal Today*. 2009;147:186-195.
26. Qi C, Huang J, Bao S, Su H, Akita T, Haruta M. Switching of reactions between hydrogenation and epoxidation of propene over Au/Ti-based oxides in the presence of H_2 and O_2. *J Catal.* 2011;281:12-20.
27. Uphade BS, Okumura M, Tsubota S, Haruta M. Effect of physical mixing of CsCl with Au/Ti-MCM-41 on the gas-phase epoxidation of propene using H_2 and O_2: drastic depression of H_2 consumption. *Appl Catal A Gen*. 2000;190:43-50.
28. Wang F, Qi C, Ma J. The study of the uncalcined Au catalyst and inorganic salts on direct gas-phase epoxidation of propylene. *Catal Commun.* 2007;8:1947-1952.
29. Qi C, Okumura M, Akita T, Haruta M. Vapor-phase epoxidation of propylene using H_2/O_2 mixture over gold catalysts supported on non-porous and mesoporous titania-silica: effect of preparation conditions and pretreatments prior to reaction. *Appl Catal A Gen.* 2004;263:19-26.
30. Uphade BS, Akita T, Nakamura T, Haruta M. Vapor-phase epoxidation of propene using H_2 and O_2 over Au/Ti-MCM-48. *J Catal.* 2002;209:331-340.
31. Stangland EE, Stavens KB, Andres RP, Delgass WN. Characterization of gold-titania catalysts via oxidation of propylene to propylene oxide. *J Catal.* 2000;191:332-337.
32. Stangland EE, Stavens KB, Andres RP, Delgass WN. Propylene epoxidation over gold-titania

catalysts. *Stud Surf Sci Catal*. 2000;130:827-832.

33. Uphade BS. Susumu T, Toshio H, Haruta M. Selective oxidation of propylene to propylene oxide or propionaldehyde over Au supported on titanosilicates in the presence of H_2 and O_2. *Chem Lett.*1998;27:1277-1278.
34. Zhuang J, Yan Z, Liu X, Liu X, Han X, Bao X, Mueller U. NMR study on the acidity of TS-1 zeolite. *Catal Lett*. 2002;83:87-91.
35. Feng X, Sheng N, Liu Y, Chen X, Chen D, Yang C, Zhou X. Simultaneously enhanced stability and selectivity for propene epoxidation with H_2 and O_2 on Au catalysts supported on nano-crystalline mesoporous TS-1. *ACS Catal*. 2017;7:2668-2675.
36. Zhu Q, Liang M, Yan W, Ma W. Effective hierarchization of TS-1 and its catalytic performance in propene epoxidation. *Micropor Mesopor Mat*. 2019;278:307-313.
37. Harris JW, Arvay J, Mitchell G, Delgass WN, Ribeiro FH. Propylene oxide inhibits propylene epoxidation over Au/TS-1. *J Catal.* 2018;365:105-114.
38. Du M, Zhan G, Yang X, Wang H, Lin W, Zhou Y, Zhu J, Lin L, Huang J, Sun D, Jia L, Li Q. Ionic liquid-enhanced immobilization of biosynthesized Au nanoparticles on TS-1 toward efficient catalysts for propylene epoxidation. *J Catal.* 2011;283:192-201.
39. Sinha AK, Seelan S, Akita T, Tsubota S, Haruta M. Vapor phase propylene epoxidation over Au/Ti-MCM-41 catalysts prepared by different Ti incorporation modes. *Appl Catal A Gen.* 2003;240:243-252.
40. Qi C, Akita T, Okumura M, Kuraoka K, Haruta M. Effect of surface chemical properties and texture of mesoporous titanosilicates on direct vapor-phase epoxidation of propylene over Au catalysts at high reaction temperature. *Appl Catal A Gen.* 2003;253:75-89.
41. Tuel A, Diab J, Gelin P, Dufaux M, Dutel J-F, Taarit YB. EPR evidence for the isomorphous substitution of titanium in silicalite structure. *J Mol Catal.* 1990;63:95-102.

42. Bal R, Chaudhari K, Srinivas D, Sivasanker S, Ratnasamy P. Redox and catalytic chemistry of Ti in titanosilicate molecular sieves: an EPR investigation. *J Mol Catal A Chem.* 2000;162:199-207.
43. Nguyen V-H, Chan H-Y, Wu JCS. Synthesis, characterization and photo-epoxidation performance of Au-loaded photocatalysts. *J Chem Sci*. 2013;125:859-867.
44. Dixon WT, Norman ROC. Free radicals formed during the oxidation and reduction of peroxides. *Nature*. 1962;196:891.
45. Liu Z, Wang T, Yu X, Geng Z, Sang Y, Liu H. In situ alternative switching between Ti^{4+} and Ti^{3+} driven by H_2O_2 in TiO_2 nanostructures: mechanism of pseudo-Fenton reaction. *Mater Chem Front.* 2017;1:1989-1994.
46. Chang E-E, Hsing H-J, Chiang P-C, Chen M-Y, Shyng J-Y. The chemical and biological characteristics of coke-oven wastewater by ozonation. *J Hazard Mater*. 2008;156:560-567.
47. Shetti VN, Manikandan P, Srinivas D, Ratnasamy P. Reactive oxygen species in epoxidation reactions over titanosilicate molecular sieves. *J Catal.* 2003;216:461-467.
48. Serrano DP, Uguina MA, Sanz R, Castillo E, Rodríguez A, Sánchez P. Synthesis and crystallization mechanism of zeolite TS-2 by microwave and conventional heating. *Micropor Mesopor Mat*. 2004;69:197-208.
49. Uguina MA, Serrano DP, Ovejero G, Grieken RV, Camacho M. TS-2 synthesis from wetness-impregnated SiO_2-TiO_2 xerogels. *Zeolites*. 1997;18:368-378.
50. Reddy JS, Kumar R. Synthesis, characterization, and catalytic properties of a titanium silicate, TS-2, with MEL structure. *J Catal.* 1991;130:440-446.
51. Laha SC, Kumar R. Highly selective epoxidation of olefinic compounds over TS-1 and TS-2 redox molecular sieves using anhydrous urea-hydrogen peroxide as oxidizing agent. *J Catal.* 2002;208:339-344.

52. Lu J, Zhang X, Bravo-Suárez JJ, Bando KK, Fujitani T, Oyama T. Direct propylene epoxidation over barium-promoted Au/Ti-TUD catalysts with H_2 and O_2: effect of Au particle size. *J Catal.* 2007;250:350-359.
53. Sinha AK, Seelan S, Tsubota S, Haruta M. A three-dimensional mesoporous titanosilicate support for gold nanoparticles: vapor-phase epoxidation of propene with high conversion. *Angew Chem Int Ed.* 2004,43:1546-1548.
54. Chen J, Halin SJA, Schouten JC, Nijhuis TA. Kinetic study of propylene epoxidation with H_2 and O_2 over Au/Ti-SiO_2 in the explosive regime. *Faraday Discuss*. 2011;152:321-336.
55. Song W, Liu Z, Liu L, Skov AL, Song N, Xiong G, Zhu K, Zhou X. A solvent evaporation route towards fabrication of hierarchically porous ZSM-11 with highly accessible mesopores. *RSC Adv.* 2015;5:31195-31204.
56. Zhang Y, Zhu K, Zhou X, Yuan W. Synthesis of hierarchically porous ZSM-5 zeolites by steam-assisted crystallization of dry gels silanized with short-chain organosilanes. *New J Chem.* 2014;38:5808-5816.
57. Tao H, Li C, Ren J, Wang Y, Lu G. Synthesis of mesoporous zeolite single crystals with cheap porogens. *J Solid State Chem*. 2011;184:1820-1827.
58. Serrano DP, Sanz R, Pizarro P, Peral A, Moreno I. Improvement of the hierarchical TS-1 properties by silanization of protozeolitic units in presence of alcohols. *Micropor Mesopor Mat.* 2013;166:59-66.
59. Feng X, Chen D, Zhou X. Thermal stability of TPA template and size-dependent selectivity of uncalcined TS-1 supported Au catalyst for propene epoxidation with H_2 and O_2. *RSC Adv.* 2016;6:44050-44056.
60. Lu J, Zhang X, Bravo-Suárez JJ, Bando KK, Fujitani T, Oyama T. Direct propylene epoxidation over barium-promoted Au/Ti-TUD catalysts with H_2 and O_2: effect of Au particle

size. *J Catal.* 2007;250:350-359.

61. Lu J, Zhang X, Bravo-Suárez JJ. Tsubota S, Gaudet J, Oyama T. Kinetics of propylene epoxidation using H_2 and O_2 over a gold/mesoporous titanosilicate catalyst. *Catal Today.* 2007;123:189-197.
62. Chen J, Halin SJA, Schouten JC, Nijhuis TA. Kinetic study of propylene epoxidation with H_2 and O_2 over Au/Ti-SiO_2 in the explosive regime. *Faraday Discuss*. 2011;152:321-336.
63. Sheng N, Liu Z, Song Z, Lin D, Feng X, Liu Y, Chen X, Chen D, Zhou X, Yang C. Enhanced stability for propene epoxidation with H_2 and O_2 over wormhole-like hierarchical TS-1 supported Au nanocatalyst. *Chem Eng J.* 2018.https://doi.org/10.1016/j.cej.2018.09.115.
64. Hao Y, Liu R, Meng X, Cheng H, Zhao F. Deactivation of Au/TiO_2 catalyst in the hydrogenation of o-chloronitrobenzene in the presence of CO_2. *J Mol Catal A: Chem.* 2011;335:183-188.
65. Engelhard H, Schaefer JA, Stietz F, Goldmann A. Interaction of gold with InP(100)4×2 surfaces. *Surf Sci.* 1992;276:21-26.
66. Rankin RB, Greeley J. Trends in selective hydrogen peroxide production on transition metal surfaces from first principles. *ACS Catal*. 2012;2:2664-2672.
67. Sun K, Kohyama M, Tanaka S, Takeda S. A Study on the mechanism for H_2 dissociation on Au/TiO_2 catalysts. *J Phys Chem C.* 2014;118:1611-1617.
68. Tang Y, Zhang Z, Lu M, Chen B, Fu W, Gan J, Qian G, Duan X, Zhou X. Site-dependent activity and selectivity of H_2O_2 formation from H_2 and O_2 over Au-based catalysts. *Ind Eng Chem* Res. 2019;58:15119-15126.
69. Xiong L, Li J, Yang B, Yu Y. Ti^{3+} in the surface of titanium dioxide: Generation, properties and photocatalytic application. *J Nanomater.* 2012;2012:1-13.
70. De Yoreo JJ, Gilbert PU, Sommerdijk NA, Penn RL, Whitelam S, Joester D, Zhang H, Rimer,

JD, Navrotsky A, Banfield JF, Wallace AF, Michel FM, Meldrum FC, Cölfen H, Dove PM. Crystallization by particle attachment in synthetic, biogenic, and geologic environments. *Science*. 2015;349:aaa6760.

71. Yoshiya M, Oyama T. Impurity and vacancy segregation at symmetric tilt grain boundaries in Y_2O_3-doped ZrO_2. *J Mater Sci*. 2011;46:4176-4190.
72. Ye G, Sun Y, Guo Z, Zhu K, Liu H, Zhou X, Coppens M-O. Effects of zeolite particle size and internal grain boundaries on Pt/Beta catalyzed isomerization of n-pentane. *J Catal.* 2018;360:152-159.